

Nonlinear finite element analysis of strength and durability of reinforced concrete and composite structures

A. Ghani Razaqpur ^{a,*}, O. Burkan Isgor ^b, Afshin Esfandiari ^c

- ^a Department of Civil Engineering, McMaster University, Hamilton, Ontario L8S 4L8, Canada
- ^b Department of Civil and Environmental Engineering, Carleton University, Ottawa, Ontario K1S 5B6, Canada
- ^c Department of Civil Engineering, University of British Columbia, Vancouver, British Columbia V6T 1Z4, Canada

ABSTRACT

The finite element method has emerged as the most powerful and versatile numerical method for solving a wide range of physical problems in science and engineering. Today a large number of commercial programs exist that can be used to solve diverse problems in structural and fluid mechanics, heat transfer and many other phenomena. However, certain critical problems related to durability of concrete structures, especially corrosion of reinforcement, cannot be readily solved using the available software. This paper presents two finite element formulations, developed by the writers, one dealing with the nonlinear analysis of composite concrete-steel bridges, and the other with the durability of concrete structures, with emphasis on the corrosion of reinforcement. The validity and accuracy of the proposed models are demonstrated by comparing their results with appropriate experimental data.

ARTICLE INFO

Article history:
Received 31 July 2015
Accepted 7 September 2015

Keywords:
Finite element method
Nonlinear analysis
Composite structures
Durability
Corrosion

1. Introduction

The finite element method (FEM) was developed nearly half a century ago (Turner et al., 1956) to solve two dimensional stress analysis problems; since then it has evolved as the most powerful numerical method for the solution of a wide range of problems in many areas of science and engineering (Zienkiewicz and Taylor, 1989). Today it is routinely used by many practicing engineers to solve diverse problems which cannot be otherwise solved due to their complex boundary conditions or anisotropic and nonlinear properties. While existing commercial software can be used to solve a wide spectrum of problems, certain practical problems in civil engineering, such as those dealing with durability of concrete structures, cannot be solved readily using current commercial software. Among these are the prediction of alkali-aggregate reaction, sulphate attack, and corrosion of reinforcement. In this paper, a summary of the basic FEM formulation for two problems that the writers have worked on will be presented. The two problems are among topics of current interest in the structural engineering community; namely, durability, serviceability and safety of concrete bridges and other exposed structures.

2. Nonlinear Analysis of Composite Bridges

Due to the noticeable increase in the permissible live load of bridges over the last 50 years, there is need for the accurate assessment of their serviceability and strength. Composite bridges, comprising steel girders attached to a concrete slab, Fig. 1(a), are common in many countries, and their serviceability and strength depend on the interaction between the concrete slab and the steel girders. Various types of connectors can be used to attach the slab to the girders, including welded steel sections and headed studs, Fig. 1(b), but today the latter type of connector is most commonly used. These connectors may achieve different levels of composite action, varying from practically no interaction to full composite action. The level of interaction may also depend on level of applied load on the bridge. Although the FEM analysis of such bridges can be performed under the assumption of full composite action, the analysis of partial interaction, caused by relative movement at the slab-girder interfaces requires more effort. Continuum contact elements, available in some FEM commercial programs, can be used to model the interaction, but the model parameters need to be carefully selected by transforming the

^{*} Corresponding author. Tel.: +1-905-525-9140; E-mail address: razaqpu@mcmaster.ca (A. G. Razaqpur) ISSN: 2149-8024 / DOI: http://dx.doi.org/10.20528/cjsmec.2015.09.030

properties of the connector to equivalent properties that can characterize the interface. Alternatively, a discrete element can be developed whose properties could be directly obtained from the geometry and material properties of the actual connector. Razaqpur and Nofal (1989) originally developed such a discrete element, which was subsequently improved by Esfandiari (2001) and its accuracy was verified by comparing its results with several sets of experimental data. The improved model and its verification are described below.





Fig. 1. (a) Typical steel-concrete composite bridge, (b) Steel girder with stud shear connectors.

2.1. Shear connector finite element

Shear connectors, as shown in Fig. 2(a), can be modeled as truss element with five degrees of freedom, where the usual sixth degree of freedom is constrained by assuming the connector to be axially rigid. This constraint is optional, but if not enforced the connector would allow for separation normal to the slab-girder interface. The derivation of the stiffness matrix for this element requires the shear force-slip relationship of the connector. One such relationship was proposed by Yam and Chapman (1968) based on their test data, viz.

$$F = a(1 - e^{-b\lambda}), \tag{1}$$

where F is the shear force acting on either end of the connector in one of the two orthogonal directions (kN) and λ (mm) is the corresponding relative displacement or slip in the direction of F, Fig. 2(b); a and b are experi-

mental constants, which depend on the connector geometry and strength; and e is base of the natural logarithm. For stud connectors, Yam and Chapman suggested a and b to be 30 kN and 4.72 mm. Using these values, Eq. (1) is plotted in Fig. 3. Note that assuming different values for a and b allows one to model connectors with different strength and stiffness.

Using Eq. (1) and assuming that shear connectors only allow slip at the interface, the stiffness matrix can be written as:

$$[K] = \begin{bmatrix} k_1 & 0 & -k_1 & 0 & 0\\ 0 & 0 & 0 & 0 & 0\\ 0 & 0 & k_2 & 0 & -k_2\\ -k_1 & 0 & 0 & k_1 & 0\\ 0 & 0 & -k_2 & 0 & k_2 \end{bmatrix}, \tag{2}$$

where k_1 and k_2 are the shear stiffness coefficients in the two orthogonal directions in the plane of the connector cross-section, and are given by

$$k_j = \frac{\partial k_j}{\partial \lambda_j} = abe^{-b\lambda},\tag{3}$$

where F_j is the component of shear force acting on the connector cross-section in direct j(j=1,2) and λ_j is its associated slip (Fig. 2(b)). As stated earlier, the bar is assumed to be axially rigid, which is enforced by imposing equal axial displacement at the two ends of the element as shown in Fig. 2(a).

In using the above stiffness matrix, there is another problem which must be considered. As illustrated in Fig. 2(b) the shear forces acting on a shear connector equilibrate each other ($\sum F_x = 0$, $\sum F_y = 0$), but they create unbalanced moments F_1L and F_2L , where L is the connector length, and these moments violate the equilibrium requirement. To overcome this problem, in this study the unbalanced moments are reversed and applied as nodal forces at the end of each iteration during the solution process (Esfandiari, 2001). These moments are

$$(dM_1)_i = (K)_{i-1} (d\lambda_1)_i L,$$
 (4a)

$$(dM_2)_i = (K)_{i-1} (d\lambda_2)_i L,$$
 (4b)

where $(dM_1)_i$ and $(dM_2)_i$ are unbalanced moments for ith iteration, $(K_1)_{i-1}$ and $(K_2)_{i-1}$ are stiffness elements of shear connector corresponding to the results of previous iteration and $(d\lambda_1)_i$, $(d\lambda_2)_i$ are incremental slip values. Note that

$$\lambda_1 = u_4 - u_1 \,, \tag{5a}$$

$$\lambda_2 = u_3 - u_5 \,, \tag{5b}$$

$$d\lambda_1 = du_1 - du_4 \,, \tag{6a}$$

$$d\lambda_2 = du_3 - du_5 \,, \tag{6b}$$

where u_j and du_j are, respectively, the total and incremental displacement of the *j*th degree of freedom.

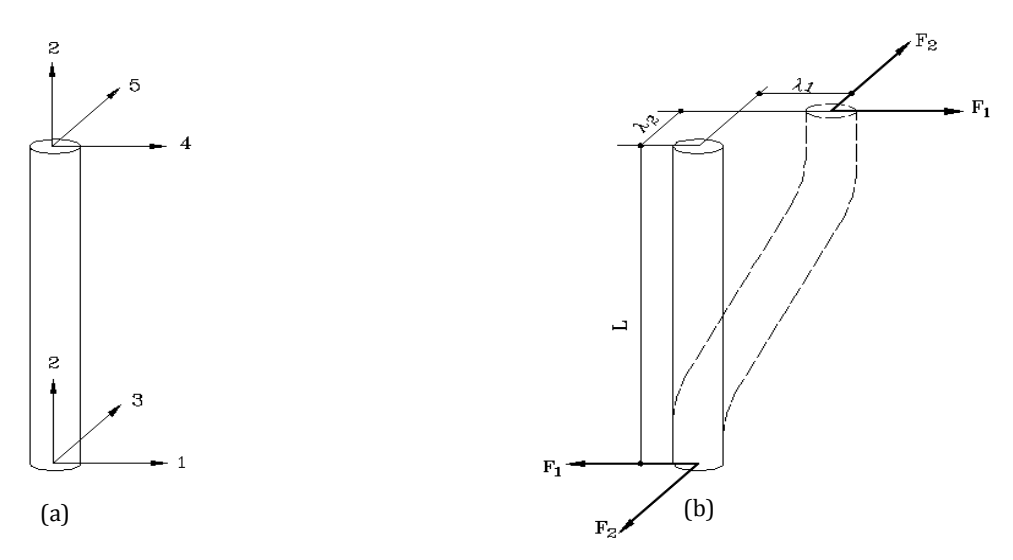


Fig. 2. Shear connector element; (a) Nodal degrees of freedom, (b) Deformed shape.

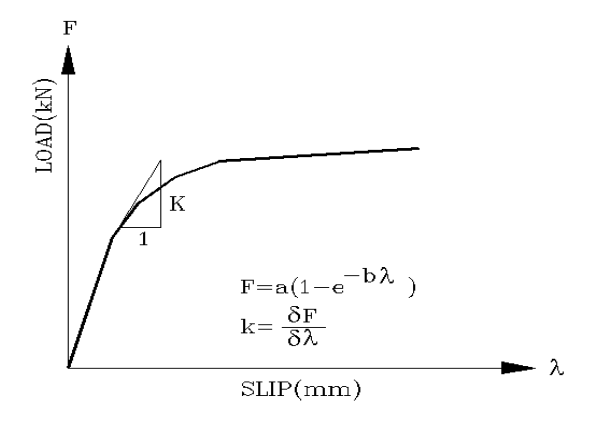


Fig. 3. Typical load slip curve for shear connector element.

2.2. Experimental verification of the model

To verify the above method, the experimental results of Yam and Chapman's continuous beam (1972), tested at Imperial College, and Razaqpur and Nofal's bridge model (1988) will be compared with the finite element results. This element is implemented in the nonlinear finite element program NONLACS (Razaqpur and Nofal, 1990), which can be used to analyze any three dimensional reinforced/prestressed concrete, steel or composite structure that can be idealized as an assemblage of thin shell elements. The program uses theory of plasticity in conjunction with Von Mises' yield criterion for the steel elements and the so-called equivalent strain concept and the Kupfer and Gerstle (1973) biaxial failure criterion for concrete. Steel reinforcement is modeled as either discrete truss bars or as smeared steel layer. The program uses the smeared crack approach and includes tension stiffening.

2.2.1. Imperial College continuous beam

Yam and Chapman reported the experimental data for a number of continuous beams. One of those beams, analyzed in this study, had the loading and geometry illustrated in Fig. 4 and the material properties shown in Table 1. The beam has two spans of 3.355 m each and consists of a 152 mm deep I-section attached to a 60 mm thick and 920 mm wide concrete slab by means of stud shear connectors. The properties in Table 1 were taken from Yam and Chapman's report, but some properties that were not given by them had to be assumed. The finite element mesh was similar to the one used for the bridge model of Razaqpur and Nofal that will be described in the next section.

Figs. 5, 6, and 7 compare the experimental and computed deflected shape, slip along concrete-steel interface, and strain along the bottom flange of the girder from the left support to the centerline at load P=108.5 kN. We see good agreement between the two sets of results, which corroborate the accuracy of the proposed model.

2.2.2. Razaqpur and Nofal bridge model

This 1/3 scale bridge model was built and tested by Razaqpur and Nofal (1988). It was the model of a two-lane bridge, 6.24 m wide and 18.00 m long. It has three W840 x 170 compact steel girders spaced at 1.86 m. The concrete slab has a total thickness of 182mm. Figs. 8 and 9 show the geometry and loading of the bridge model and Table 2 shows its material properties. The material strength values were obtained by Razaqpur and Nofal from ancillary tests performed on concrete cylinders and steel coupons. The bridge is simply supported with three girders (3 W250x39) on 6 m span. The supports are roller at one end and hinged at the other and the slab is 70 mm thick and 2060 mm wide.

The actuator loads were applied through $83\ mm\ x\ 200\ mm$ steel plates, placed above the central girder flange on the concrete slab.

2.2.3. Finite element idealization

The finite element idealization of the bridge is shown in Fig. 10. The finite element mesh consists of 20 elements along the span and 24 in the cross section. The top and bottom steel reinforcement in the slab was modeled

as smeared layers, and the slab mid-plane nodes were connected to the top flange nodes directly below them by the shear connector elements. As shown in Fig. 10, the steel girders webs and flanges were idealized by elements with a

single layer, while the concrete slab was divided into 10 layers through its thickness. The applied load was divided into 20 increments and the bridge was analyzed over the entire loading range up to failure.

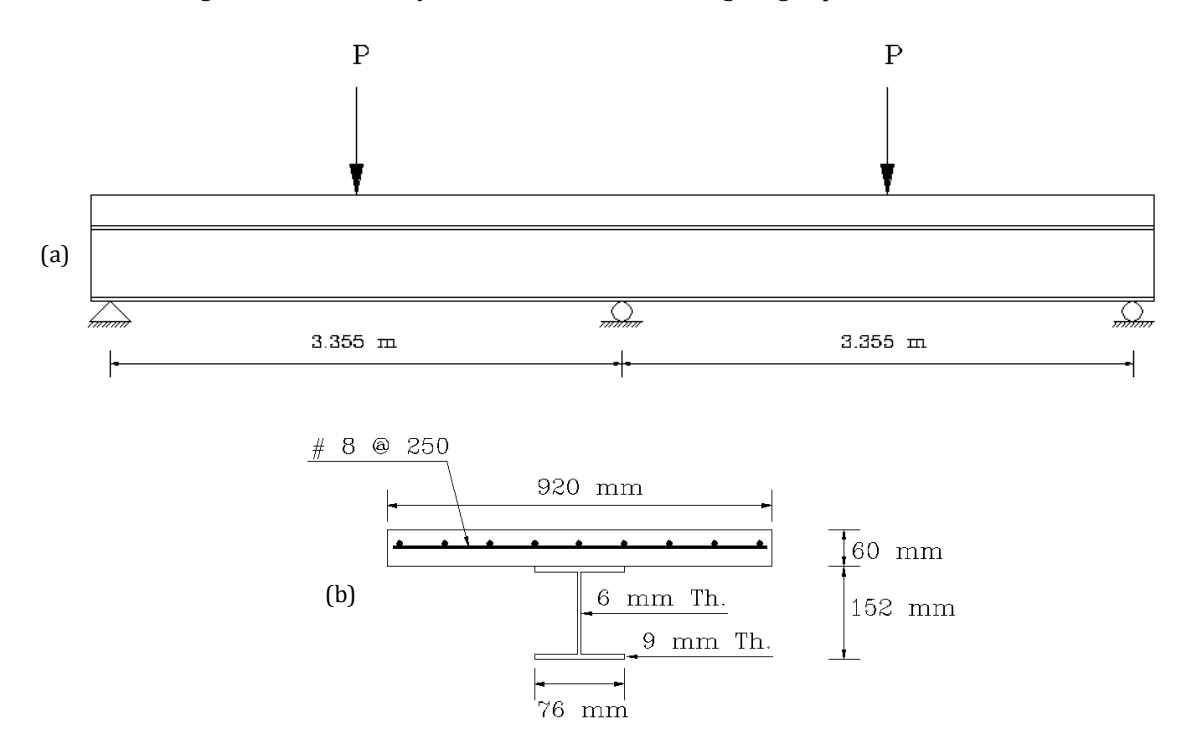


Fig. 4. Imperial College continuous beam details; (a) Elevation, (b) Cross section.

Table 1. Material properties of Imperial College continuous beam.

Material Constants	Concrete	Reinforcing Steel	Steel Girder	
f_y (MPa)	-	270	270	Given
E_s (MPa)	-	200000	200000	Given
E_{s}^{*} (MPa)	-	5000	5000	Given
f'_c (MPa)	47.6	-	-	Given
\mathcal{E}_{max}	0.035	-	-	Assumed
€ cu	0.002	-	-	Assumed
Connector Details $\frac{3'}{8} \times 2'$ Headed studs, two rows at 5.72 inch				

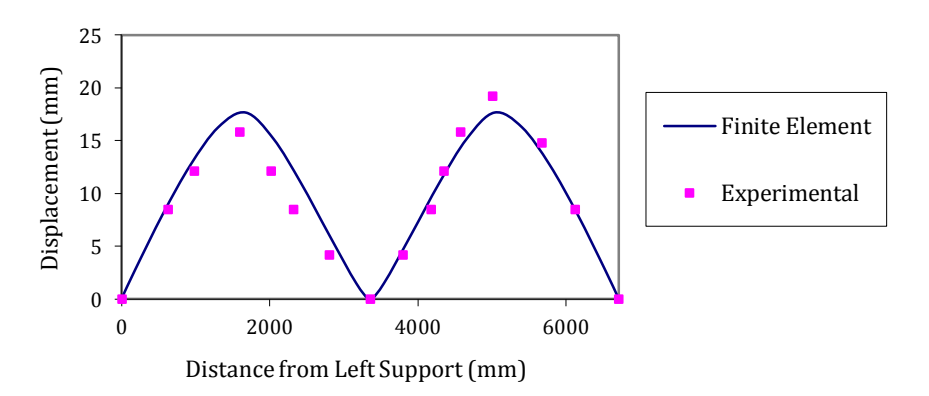


Fig. 5. Deflected shape of Imperial College continuous beam at *P*=108.5 kN.

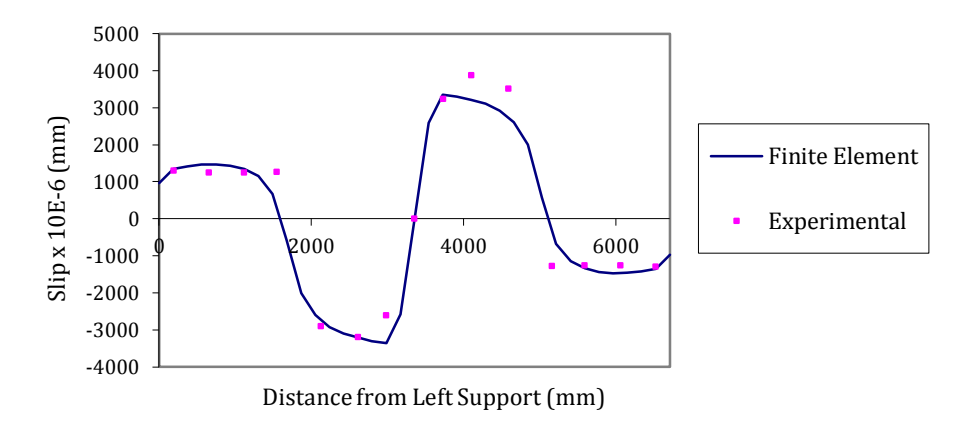


Fig. 6. Concrete-steel interface slip in continuous beam at *P*=108.5 kN.

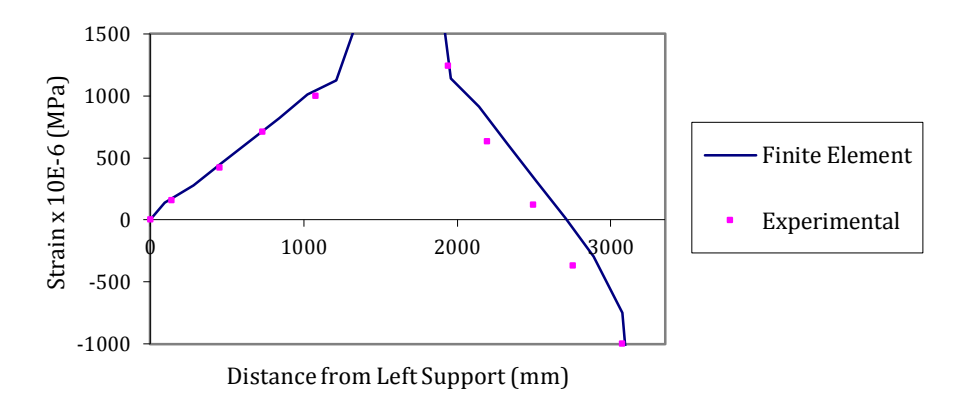


Fig. 7. Strain along the bottom flange of the continuous beam at *P*=108.5 kN.

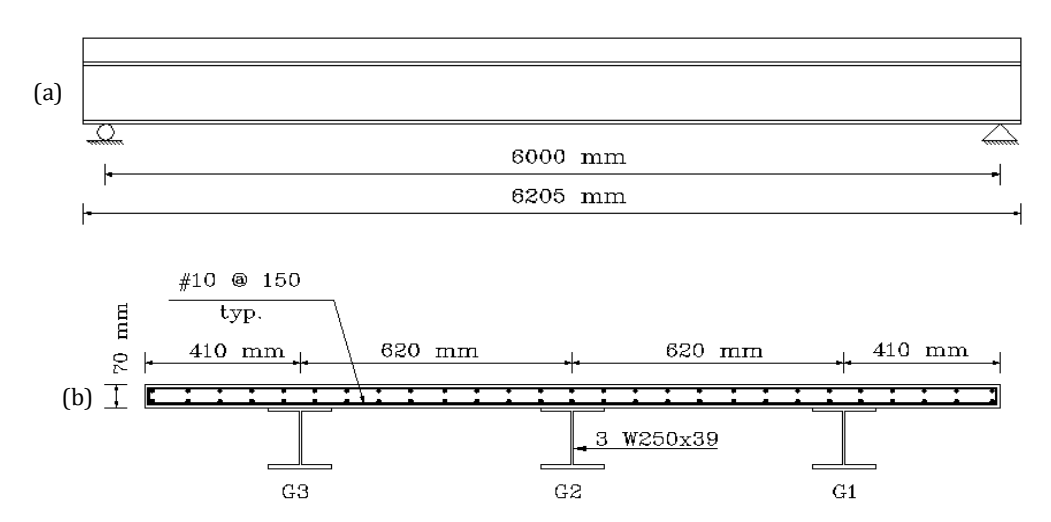


Fig. 8. Geometry of bridge model; a) Elevation, b) Cross section.

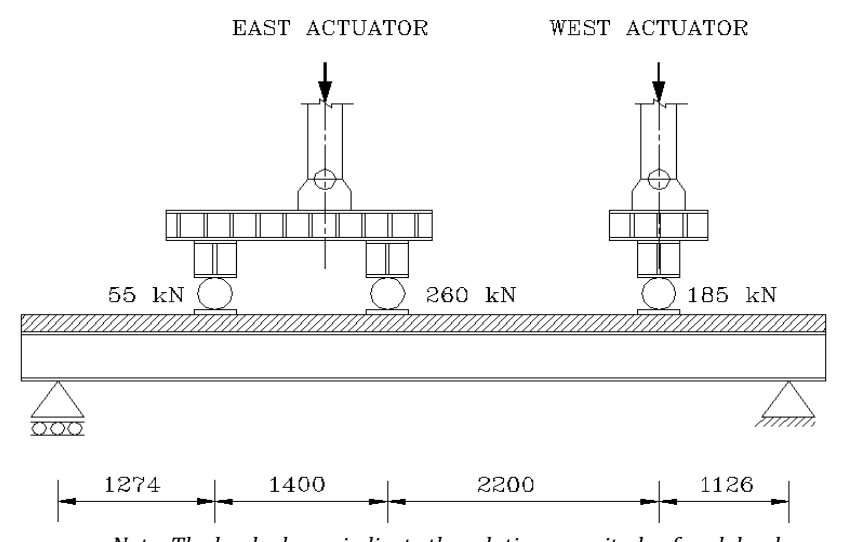
2.2.4. Comparison of FEM results with experimental data

For brevity, selective FEM results are compared with the corresponding experimental data. Fig. 11(a) shows the full load- deflection curve of Girder 3 while Fig. 11(b) shows the deflected shape of the same girder under increasing load. The ultimate load predicted by finite element was calculated to be 800 kN, which is 4% higher than the corresponding experimental load of 766 kN.

Actually, the test had to be stopped because the actuator stroke was exhausted, albeit at the end of the test,

large deformations and a visible plastic hinge had formed in the central girder. Thus, it is possible that the bridge could still carry some extra load before total collapse.

The variation of the longitudinal strain along the centerline of the top and bottom flanges of Girder G3 is plotted for different load levels in Fig. 12(a) and (b), respectively. Considering the rather large strain values in the bottom flange, it is obvious that the bridge has practically reached its ultimate capacity and is on the verge of failure. Similarly good comparison was observed for the concrete and steel reinforcement strains.



 $Note: The \ loads \ shown \ indicate \ the \ relative \ magnitude \ of \ each \ load$

Fig. 9. Loading of bridge model.

Table 2. Material properties of bridge model.

Material Constants	Concrete	Reinforcing Steel	Steel Girder	
f _y (MPa)	-	400	300	Given
E_s (MPa)	-	200000	200000	Given
E_{s}^{*} (MPa)	-	0	0	Given
f_c' (MPa)	40	-	-	Given
ε_{max} (at peak stress)	0.002	-	-	Assumed
\mathcal{E}_{cu} (at peak failure)	0.0035	-	-	Assumed
Connector Details $15 \text{ mm} \times 60 \text{ mm}$ Headed studs, two rows at 150 mm				

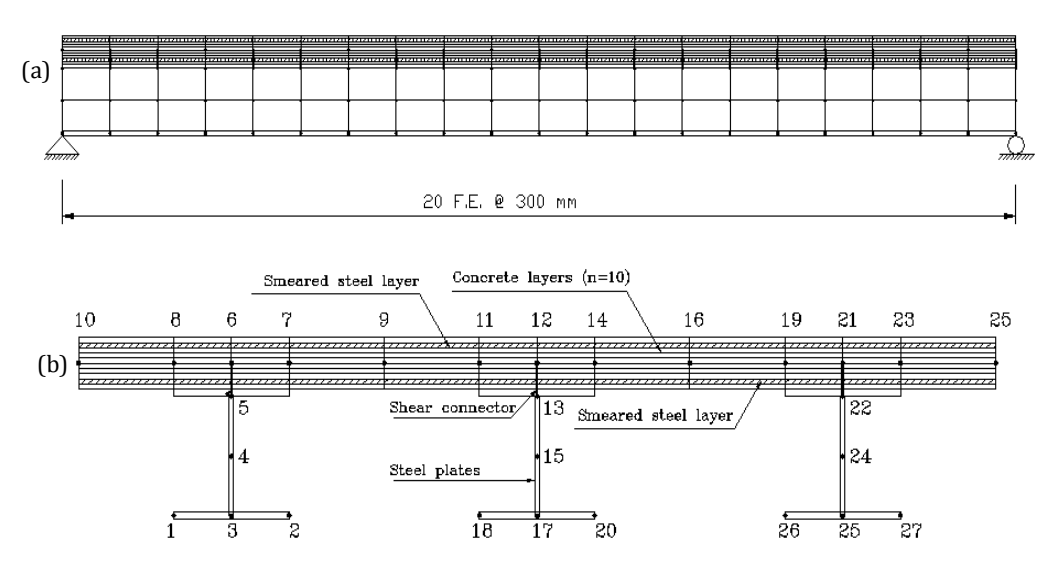


Fig. 10. Finite element idealization of bridge model; a) Elevation, b) Cross section.

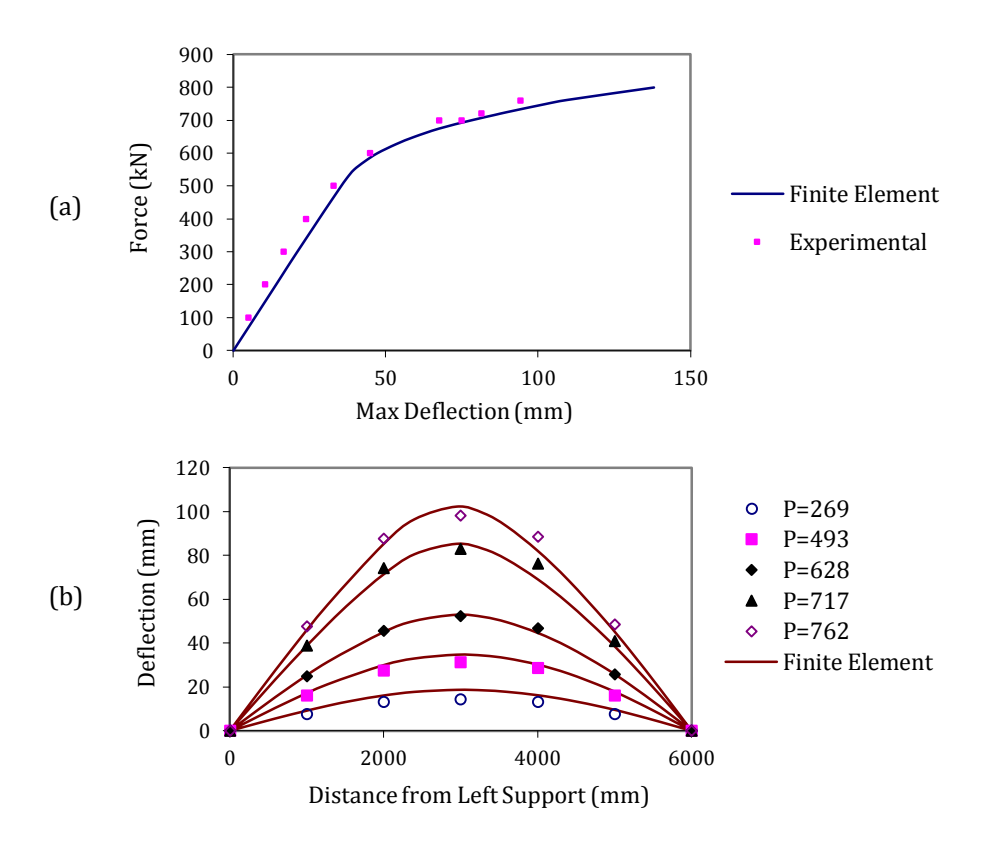


Fig. 11. Comparison of FEM and experimental results for girder G3; (a) Load-maximum deflection curve, (b) Deflected shape.

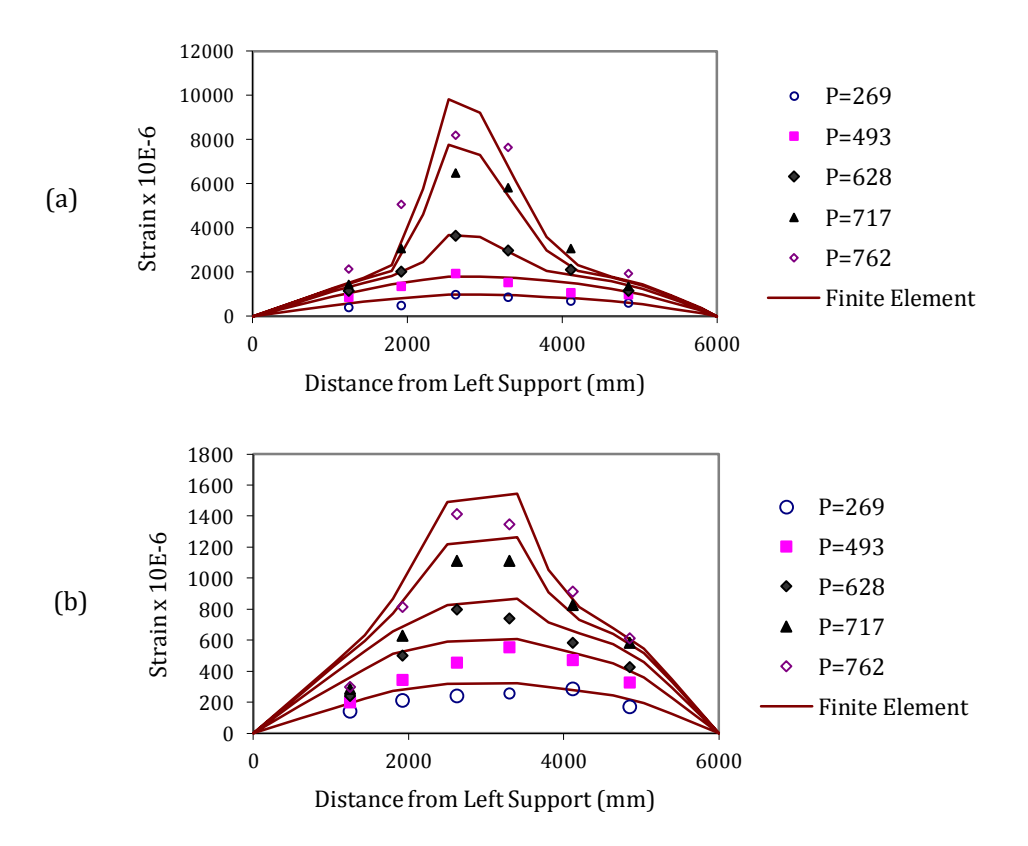


Fig. 12. Comparison of girder G3 top and bottom flanges longitudinal strain values obtained by FEM analysis with the corresponding experimental data; (a) Top flance, (b) Bottom flance.

Again, it is clear that program NONLAC and the proposed shear connector model predicts the response of these bridges accurately.

Next, the finite element formulation of chloride diffusion, carbonation and reinforcement corrosion in concrete structures is presented.

3. FEM Modelling of Concrete Durability

To prevent steel reinforcement corrosion and the ensuing deterioration of concrete, it is useful to have tools that would enable designers to predict the performance of structures under prescribed environmental/chemical conditions. Here a model is proposed and is implemented in a finite element program. The results of the model are validated by comparing them with available experimental data. The model includes consideration of the various phenomena which influence both the initiation and propagation stages of the corrosion process. This includes temperature, moisture, chloride ions, and oxygen transport within concrete. The model accounts for the effects of changes in exposure conditions on the rate of corrosion and the effects of the corrosion reactions on the transport properties of concrete.

3.1. Steel reinforcement corrosion process

Within the initially high alkaline environment of concrete, reinforcing steel is covered with an insoluble film of iron oxides (passive layer) which normally protects the steel from further corrosion. The loss of the passive layer, termed depassivation, leads to further corrosion. The presence of chloride ions, the carbonation of concrete, the physical and the chemical properties of concrete, the surface characteristics and the chemical composition of steel, and sustained mechanical stresses are key factors influencing the depassivation and rate of corrosion of steel in concrete (Neville, 1996; Broomfield, 1997; Uhlig and Revie, 1985).

It has become common practice to divide the corrosion process in concrete into two successive stages. The first stage, called the initiation stage, is defined as the period during which corrosive agents, such as chloride ions or carbon dioxide, enter concrete and move towards the reinforcement from the surface of concrete, while the steel remains passive. The loss of passivity marks the onset of the second, or propagation, stage during which active corrosion of steel occurs (Tutti, 1982). Existing models define the beginning of the propagation stage in terms of the free chloride concentration at the surface of the steel. Once this concentration exceeds a prescribed threshold, corrosion is assumed to commence. Subsequent entry of more chlorides is assumed to be inconsequential insofar as corrosion rate and amount is concerned. The problem with this approach is neglecting the symbiotic relationship between the initiation and propagation stages (Maruya et al., 2003).

In the present study, which is based on the writer's previous work (Isgor and Razaqpur, 2004, 2005, 2006a

and 2006b), the initiation and propagation stages are unified and are treated with the same level of detail. In existing models, the initiation stage parameters, such as concrete temperature, moisture content, chloride ions and oxygen concentrations normally vary within this stage, but not in the propagation stage. On the contrary, in the proposed model these parameters are assumed to vary in both stages, which allows for the consideration of the effects of corrosion reactions on the properties of concrete and the chemical composition of the pore solution around the reinforcement (e.g. changes in electrical resistivity, pH, and oxygen concentration).

3.2. Proposed model

As discussed previously, the proposed model consists of initiation and propagation stages as described below.

3.2.1. Initiation stage

The governing equations of the phenomena considered in the initiation stage of the model are shown in Table 3. Fig. 13 illustrates the solution strategy that is used, and it allows the distribution of the following environmental / chemical quantities in a member: temperature, moisture, pH (OH- concentration), and oxygen concentration.

3.2.2. Finite element solution of governing equations

As indicated in Table 3, the distribution of each parameter in concrete is governed by a quasi-harmonic equation of the form:

$$k_x \frac{\partial^2 \phi}{\partial x^2} + k_y \frac{\partial^2 \phi}{\partial y^2} + Q = m \frac{\partial \phi}{\partial t},\tag{7}$$

where k_x and k_y are the appropriate conductivities, Q is the sink/source term, and m is a coefficient representing the pertinent material properties. The quantity φ denotes a potential which may be due to chemical concentration, thermal, electrical or hydraulic fields. The term on the right-hand side of Eq. (7) represents the change in potential with time. Following Logan (1992), the functional corresponding to Eq. (7) may be written as π_b :

$$\pi_{h} = \frac{1}{2} \iiint_{V} \left[k_{x} \left(\frac{\partial \varphi}{\partial x} \right)^{2} + k_{y} \left(\frac{\partial \varphi}{\partial y} \right)^{2} - 2 \left(\mathcal{Q} - c \rho \frac{\partial \varphi}{\partial t} \right) \varphi \right] dV - \iiint_{S_{1}} q^{*} \varphi dS + \frac{1}{2} \iint_{S_{2}} h_{c} (\varphi - \varphi_{\infty})^{2} dS , \quad (8)$$

where h_c is the coefficient of convection, ϕ_{∞} is the value of the field variable away from the boundary, V is the volume of the domain of interest (finite element), S is its surface, S_1 and S_2 are portions of the boundary over which flux q^* , and convective transfer are specified, respectively. Using customary finite element notation, Eq. (2) can be written in matrix form as:

$$\pi_{h} = \frac{1}{2} \{\phi\}^{T} \iiint_{V} \left[[B]^{T} [D] [B] \right] dV \{\phi\} - \{\phi\}^{T} \iiint_{V} [N]^{T} Q dV + \iiint_{V} \rho c[N]^{T} \{\phi\}^{T} [N] \frac{\partial \{\phi\}}{\partial t} dV - \{\phi\}^{T} \iint_{S_{1}} [N]^{T} q * dS + \frac{1}{2} \iint_{S_{2}} h_{c} \left[(\{\phi\}^{T} [N]^{T} [N] \{\phi\} - (\{\phi\}^{T} [N]^{T} + [N] \{\phi\}) \phi_{\infty} + \phi_{\infty}^{2} \right) \right] dS,$$

$$(9)$$

where $\{\phi\}$ is the vector representing the nodal values of the field variable, [N] is the shape function matrix, [D] is the material property matrix and [B] is a matrix whose elements are derivatives of the shape functions.

Table 3. The governing equations of the initiation stage of the model.

Process	Governing Equation	Definitions	Explanations
Heat Transfer $\phi = T$	$k\nabla^2 T + Q_T = \rho c \frac{\partial T}{\partial t} + \frac{hP}{A} (T - T_{\infty})$	T : temperature k : Thermal conductivity Q_T : sink / source term ρ : density c : specific heat of concrete t : time h : coeff. of conductive heat transfer $A(P)$: area(perimeter)	Includes convective and radiative boundary conditions Assumed to be unaffected by the moisture tranfer
Moisture Transfer $\phi = h$	$D_h \nabla^2 h + Q_h = \frac{\partial w_e}{\partial h} \frac{\partial h}{\partial t}$	h : relative humidity D_h : moisture diffusion coefficient Q_h : sink / source term w_e : evaporable water content t : time	 Dh is a function of temperature Production of water in the carbonation reaction provides the source term for the moisture transfer analysis Equilibrium between vapour and liquid phases is monitored by using equilibrium isotherms
Chloride Transport $\phi = C_f$	$D_{Cl}\nabla^2 C_f + Q_{Cl} = \frac{\partial C_f}{\partial t}$	C_f : free [Cl-] D_{cl} : Chloride diffusion coefficient Q_{cl} : sink / source term representing chloride binding or release t : time	A number of Chloride binding isotherms are implemented in the model through the sink term Chloride release under low pH is implemented by using the source term
CO_2 Transport $\phi = C_c$	$D_c \nabla^2 C_c + Q_c = \frac{\partial C_c}{\partial t}$	C_c : CO ₂ concentration D_c : CO ₂ diffusion coefficient Q_c : sink / source term representing carbonation reactions t: time	1) The source term represents the carbonation reactions 2) The concentration changes of chemical compounds and the pH are monitored at each time step 3) Changes in pore structure due to carbonation is considered
O_2 Transport $\phi = C_o$	$D_o \nabla^2 C_o + Q_o = \frac{\partial C_o}{\partial t}$	$C_o: O_2$ concentration $D_o: O_2$ diffusion coefficient $Q_o: sink / source term$ t: time	1) Oxygen diffusion is considered to be a function of moisture content, temperature and porosity of concrete

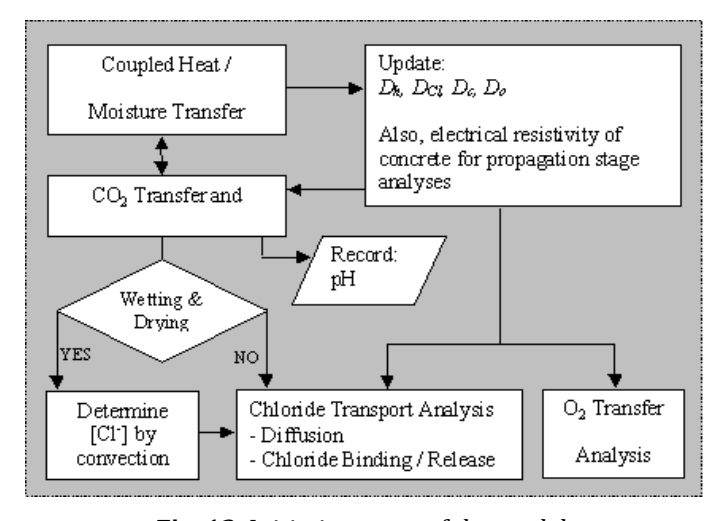


Fig. 13. Initiation stage of the model.

Using the principle of stationary potential, the following equations of equilibrium are obtained:

$$[k]\{\phi\} + [m]\{\dot{\phi}\} = \{f\},$$
 (10)

where the superscript dot denotes differentiation with respect to time. Eq. (10) can be written in expanded form as:

$$\left[\iiint_{V} \left[[B]^{T}[D][B] \right] dV + \iint_{S_{2}} h[N]^{T}[N] dS \right] \{\phi\} + \\
\left[\iiint_{V} c\rho[N]^{T}[N] dV \right] \{\dot{\phi}\} = \iiint_{V} [N]^{T} Q dV + \\
\iint_{S_{1}} [N]^{T} q^{*} dS + \iint_{S_{2}} [N]^{T} h_{c} \varphi_{\infty} dS . \tag{11}$$

Using well known finite element techniques, the global balance equations are set-up by assembling the element balance equations, and they are solved using numerical time integration schemes; the details of the solution procedure and more information on the initiation stage can be found in Martín-Pérez (1999) and Dhatt and Touzot (1984).

3.2.3. Propagation stage

The corrosion rate of steel is a function of the current density, which can be determined at any point on the steel if the electrochemical potential (abbreviated henceforth as "potential") distribution around that point is known. Knowing the potential distribution, the current density, i [A/cm²], at any point on the steel surface can be calculated using:

$$i = -\frac{1}{r} \frac{\partial \phi}{\partial n}. \tag{12}$$

 ϕ [volts] is the potential, r [Ω -cm (ohm-cm)] is the resistivity of the pore solution and n is the direction normal to the bar surface.

The rate of rust production at the anodic regions, J_{rust} [kg/m²·s], is related to the current density by Faraday's law. Consequently, the rate of ferrous oxide, Fe(OH)2, production, J_{Fa} , at the anodic regions can be written as:

$$J_{Fa} = \frac{i_a}{z_F} = 4.656 \times 10^{-7} i_a \,, \tag{13}$$

where i_a is the anodic current density, F is the Faraday's constant (9.65x10⁴ C/mol), and z is the number of electrons exchanged in the reaction (z=2 for steel corrosion). Fe(OH)₂, can be further oxidized, and this will result in the production of Fe(OH)₃. Since one mole of Fe(OH)₂, which is 89.845 g, produces one mole of Fe(OH)₃ (106.845 g), the rate of rust production, J_{rust} , at the anodic regions can be calculated as:

$$J_{rust} = \frac{106.845}{89.845} J_{Fa} = 5.556 \times 10^{-7} i_a.$$
 (14)

The main difficulty in this process is the calculation of current densities on the steel surface. According to Eq. (12), the calculation of current densities requires knowledge of the electrochemical potential distribution in the vicinity of the reinforcement.

Based on the law of electrical charge conservation and isotropic conductivity, the potential distribution can be represented by the Laplace's equation (Munn, 1982):

$$\nabla^2 \phi = 0. \tag{15}$$

To determine the potential distribution on the surface of the steel, one must solve Eq. (15) subject to prescribed boundary conditions. The boundary conditions comprise the relationship between potential and current density for the anodic and cathodic regions as well as prescribed current densities. For the anodic and cathodic regions of the steel surface, the boundary condition are defined as $\phi = \phi_a$ and $\phi = \phi_c$, where ϕ_a and ϕ_c are polarized anodic and cathodic potentials which can be expressed as (Stern and Geary, 1957):

$$\phi_a = \phi_{Fe} + \beta_a \log \frac{i_a}{i_{oa}} + i_a R_e , \qquad (16)$$

$$\phi_c = \phi_{O_2} + \beta_c \log \frac{i_c}{i_{oc}} - \frac{2.303RT}{zF} \log \frac{i_L}{i_L - i_c} + i_c R_e$$
, (17)

where ϕ^o_{Fe} and $\phi^o_{O_2}$ are the standard half-cell potentials of Fe and O₂, respectively, β_a is the Tafel slope of the anodic reaction, and i_{0a} is the anodic exchange current density, β_c is the Tafel slope of the cathodic reaction, i_{oc} is the exchange current density of the cathodic reaction, i_L is the limiting current density, and R_e is the resistance (Ohms) of the pore solution around the cathodic sites. For more information about the polarization behavior of steel, reference can be made to Uhlig and Revie (1985) and Stern and Geary (1957). The prescribed current boundary conditions on the steel surface are non-linear because current densities i_a and i_c are functions of the polarized potential, which is the state variable of Eq. (9). In the following sections, we will present our solution strategy to solve this problem in order to determine the corrosion rate in a given structure.

Eq. (15) is a special case of Eq. (7), hence the finite element formulation of Eq. (7) follows the same steps as those described for Eq. (7). However, due to the non-linear boundary conditions given by Eqs. (16) and (17), Eq. (15) must be solved by using an iterative technique.

3.2.4. Numerical example

To illustrate the accuracy of the proposed procedure, Li's (2001) experimental work is simulated. The experiment consists of a large scale beam, as illustrated in Fig. 14, exposed to a chloride solution on its top surface. To increase the concrete permeability, the beam was precracked by subjecting it to the loading shown. The exposure conditions in the test and other details of the experimental program can be obtained from Li (2001).

Using the input data given in Table 4, the corrosion rate in the top reinforcement is determined using the proposed model. The beam was discretized by 3091 four node elements. Due to space limitations, other details of the simulation are not shown, but Fig. 15(a) compares the predicted and measured half-cell potential values. While in the experiment, the actual amount of corrosion was not measured, in the simulation it was calculated as shown in Fig. 15(b). From Fig. 15(a) we can see that the simulation results are in good agreement with the experimental data.

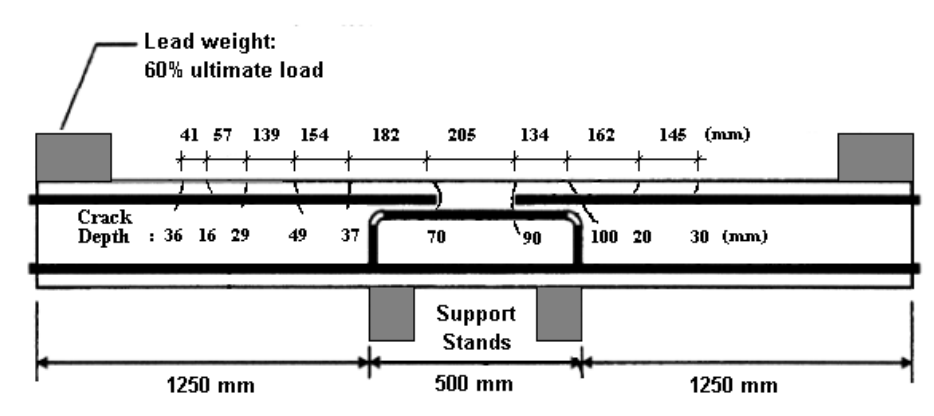


Fig. 14. Geometry and crack distribution of the modelled beam.

Table 4. Parameters used in the proposed model.

Initiation Stage Parameters	Value
Specific heat	1000 J/kg°C
Coefficient of conduction	2 W/m°C
Density of concrete	2400 kg/m^3
Adsorption isotherm	BET
Chloride binding isotherm	Langmuir
Chloride release	No release
Chloride threshold value	0.06% of concrete wt.
Propagation Stage Parameters	Value
Reference concrete resistivity	14000 Ω-cm at 25°C
Initial oxygen concentration	$0.005kg/m^3solution$
External oxygen concentration	0.0085 kg/m³ solution
Oxygen diffusion coefficient	Calculated
Fugacity of oxygen	0.2
Cathodic exchange current density	6.25 x 10 ⁻¹⁰ A/cm ²
Anodic exchange current density	1.875 x 10 ⁻⁸ A/cm ²
Thickness of the stagnant layer around the steel surface	0.05 cm
Transference number	1
Cathodic limiting current density	Calculated
Tafel slope for the cathodic reaction	Calculated
Tafel slope for the anodic reaction	Calculated

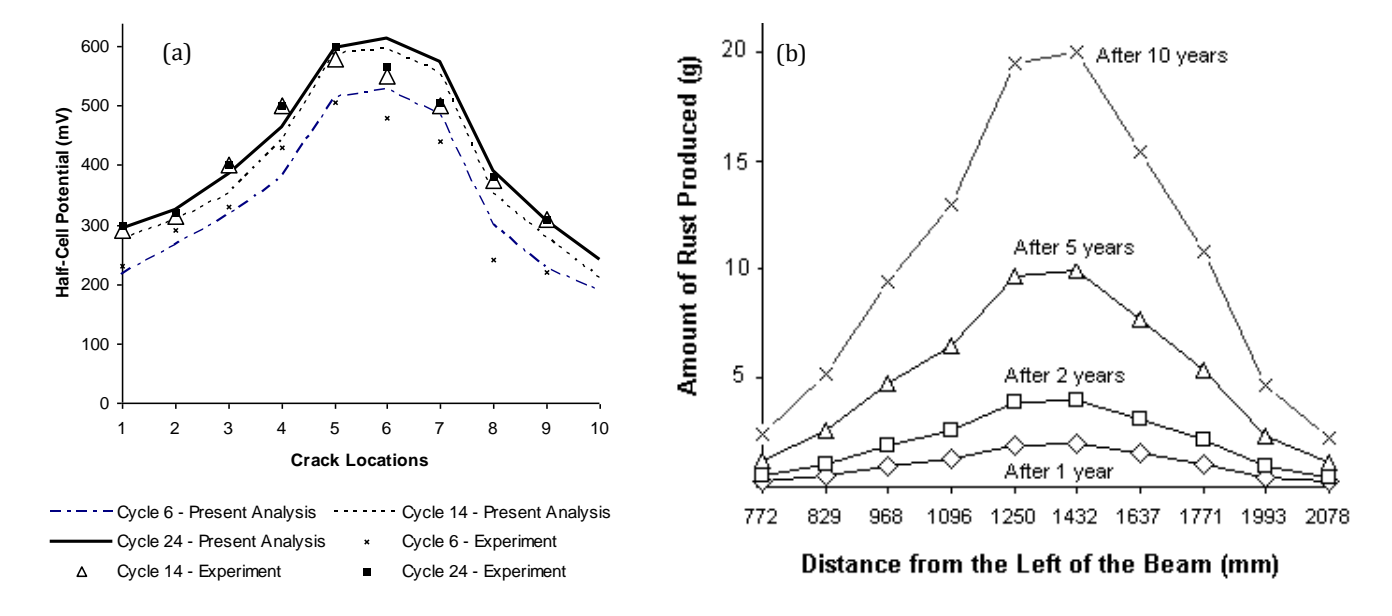


Fig. 15. (a) Comparison of the finite element analysis results for half–cell potential with the experimental data for the beam at the crack locations, (b) Predicted amount of corrosion along the top reinforcement in Li's test beam.

4. Conclusions

Two finite element modelling methods and their experimental validation are presented. The first model deals with the nonlinear response and ultimate strength capacity of composite concrete-steel bridges while the second one deals with durability of reinforced concrete structures, with particular emphasis on the corrosion of reinforcement.

The objective of the paper is to demonstrate that the utilization of suitable theoretical/empirical models, in conjunction with the powerful nonlinear finite element technique, can provide engineers with useful simulation tools, and the ability to predict the response of structures under variable loading, environmental and material degradation conditions. The current results show that although the phenomenon of corrosion in concrete is complex, nevertheless, the electrochemical principles that govern its initiation and propagation can be captured by means of numerical simulations.

REFERENCES

- Broomfield JP (1997). Corrosion of Steel in Concrete. E&FN Spon, London, UK.
- Dhatt G, Touzot G (1984). The Finite Element Method Displayed. J. Wiley & Sons, New York, USA.
- Esfandiari A (2001). Redistribution of Longitudinal Moment in Straight Continuous Concrete Slab-Steel Girder Composite Bridges. *M.Sc. thesis*, Department of Civil and Environmental Eng., Carleton University. Ottawa. Canada.
- Isgor OB, Razaqpur AG (2004). FE modelling of coupled heat transfer, moisture transport and carbonation processes in concrete structures. *Journal of Cement and Concrete Composites*, 26, 57-73.
- Isgor OB, Razaqpur AG (2005). Verification and application of a comprehensive model for predicting steel corrosion in concrete structures. *Proceedings of ConMat '05*, Vancouver, Canada.
- Isgor OB, Razaqpur AG (2006a). Advanced modelling of concrete deterioration due to reinforcement corrosion. *Canadian Journal of Civil Engineering*, 33, 707-718.

- Isgor OB, Razaqpur AG (2006b). Modelling reinforcement corrosion in concrete structures. *International Journal of Materials and Structures*, 39, 291-302.
- Kupfer H, Gerstle KH (1973). Behavior of concrete under biaxial stresses. *Journal of the Engineering Mechanics Division, ASCE*, 99(4).
- Li CQ (2001). Initiation of chloride-induced reinforcement corrosion in concrete structural members – Experimentation. ACI Structural Journal, 98(4), 502-510.
- Logan DL (1992). A First Course in Finite Element Method. PWS Publishing, Boston, USA.
- Martín-Pérez B (1999). Service Life Modeling of RC Highway Structures Exposed To Chlorides. *Ph.D thesis*, University of Toronto, Toronto, Canada.
- Maruya T, Hsu K, Takeda H, Tangtermsirikul S (2003). Numerical modelling of steel corrosion in concrete structures due to chloride ion, oxygen and water movement. *Journal of Advanced Concrete Technology*, 1(2), 147-160.
- Munn RS (1982). A mathematical model for galvanic anode cathodic protection system. *Materials Performance*, 21, 29-41.
- Neville A (1996). Properties of Concrete. 4th ed., J. Wiley & Sons, New York, USA.
- Razaqpur AG, Nofal ME (1988). Transverse load distribution at ultimate limit states in single span slab on girder bridges with compact steel girders. Final Report, Proj: 23182, Ministry of Transportation of Ontario, Downsview, Ontario.
- Razaqpur AG, Nofal M (1989). A finite element for modeling the nonlinear behavior of shear connectors in composite structures. *Journal of Computers and Structures*, 32(1), 169-174.
- Razaqpur AG, Nofal M (1990). Analytical modeling of nonlinear behavior of composite bridges. *Journal of Structural Engineering*, ASCE, 116(6), 1715-1733.
- Stern M, Geary AL (1957). Electrochemical polarization: a theoretical analysis of the shape of the polarization curves. *Journal of the Electrochemical Society*, 104(1), 56-63.
- Turner MJ, Clogh RW, Martin HC, Topp LJ (1956). Stiffness and deflection analysis of complex structures. *Journal of Aeronautical Science*, 23, 805-823.
- Tuutti K (1982). Corrosion of Steel in Concrete. Technical Report, Swedish Cement and Concrete Research Institute, Stockholm.
- Uhlig HH, Revie RW (1985). Corrosion and Corrosion Control. 3rd ed., J. Wiley & Sons, New York, USA.
- Yam LCP, Chapman JC (1972). The inelastic behavior of continuous composite beams of steel and concrete. *Proceedings, Institute of Civil Engineers*, 53, 487-501.
- Zienkiewicz OC, Taylor RL (1989). The Finite Element Method. Vol. 2, 4th ed., McGraw-Hill International, UK.